Power dissipation, gas temperatures and electron densities of cold atmospheric pressure helium and argon RF plasma jets

Power dissipation, gas temperatures and electron densities of cold atmospheric pressure helium and argon RF plasma jets

2011 Plasma Sources Sci. Technol. 20 065010

(http://iopscience.iop.org/0963-0252/20/6/065010)

Plasma Sources Sci. Technol. **20** (2011) 065010 (12pp) doi:10.1088/0963-0252/20/6/065010

Power dissipation, gas temperatures and electron densities of cold atmospheric pressure helium and argon RF plasma jets

S Hofmann, A F H van Gessel, T Verreycken and P Bruggeman

Eindhoven University of Technology, Department of Applied Physics, PO Box 513, 5600 MB Eindhoven, The Netherlands

E-mail: s.hofmann@tue.nl

Received 15 June 2011, in final form 26 October 2011
Published 29 November 2011
Online at stacks.iop.org/PSST/20/065010

Abstract

A set of diagnostic methods to obtain the plasma parameters including power dissipation, gas temperature and electron density is evaluated for an atmospheric pressure helium or argon radio frequency (RF) plasma needle for biomedical applications operated in open air. The power density of the plasma is more or less constant and equal to 1.3×10^9 W m^{-3}. Different methods are investigated and evaluated to obtain the gas temperature. In this paper the gas temperatures obtained by rotational spectra of OH(A–X) and N_2^+ (B–X) are compared with Rayleigh scattering measurements and measurements of the line broadening of hydrogen and helium emission lines. The obtained gas temperature ranges from 300 to 650 K, depending on the gas. The electron densities are estimated from the Stark broadening of the hydrogen α and β lines which yield values between 10^{19} and 10^{20} m^{-3}. In the case of helium, this is an overestimate as is shown by a power balance from the measured power density in the plasma jet. The obtained plasma parameters enable us to explain the radial contraction of the argon plasma compared with the more diffuse helium plasma. The accuracy of all considered diagnostics is discussed in detail.

(Some figures may appear in colour only in the online journal)

1. Introduction

Non-thermal atmospheric pressure plasma jets (APPJs) are used for a wide range of surface treatment applications. Due to electron temperatures of a few electron volt (eV) APPJs are able to create reactive and charged species, metastable atoms and UV photons. This and the fact that APPJs can be operated close to room temperature is promising for biomedical applications such as inactivation of bacteria and wound treatment [1–3].

Different electrode configurations are developed in the past ranging from parallel-plate to concentric electrode configurations. Depending on the application, dc-pulsed, radio frequency (RF) or microwave (MW) is used to create a discharge. The sizes of typical APPJs range from a few millimetres to a few centimetres [3–7].

To get a better insight of the plasma-bio interaction, characterization of the plasma source in terms of gas temperature, electron density (n_e) and absorbed power is an important but non-trivial task. Non-trivial as the gas temperature has to be below 42 °C to prevent cell destruction [8] and very accurate gas temperature measurements are thus required. The same arguments holds for the power dissipation as at low power dissipation in the plasma the power dissipation in the matching box becomes non-negligible. At small electron densities line broadening measurements are more complex because other broadening mechanisms than Stark broadening become dominant (see further).

The power dissipation of the plasma is a basic physical property of the plasma which can almost directly lead to estimates of n_e. One method to obtain the power of RF plasmas is to use commercial thermal power meters. However, in this method power dissipation of the matching box is an important factor as it can be bigger than the power dissipation in the plasma. Additionally these methods are often not applicable for time-dependent power measurements, e.g. for pulsed RF signals [9].

Voltage and current probes can be directly connected to the electrodes, allowing us to calculate the power dissipation of the plasma [10, 11]. In the case of APPJs, however, the capacity of the probes is in the same order of magnitude as the capacity of the source. Due to this and the large resistance of the source, the introduction of the probe influences the impedance of the circuit significantly [12].

For biomedical applications such as wound treatment, the gas temperature has to be close to room temperature. To measure the gas temperature optical emission spectroscopy is an often used non-invasive method [13, 14]. The rotational spectrum of molecules such as OH, N_2, N_2^+ is widely used for temperature determination. However, in this case the rotational states should follow a Boltzmann distribution, which is for atmospheric pressure plasmas in most conditions the case but not in general as work of Bruggeman *et al* [15] has shown with atmospheric pressure plasmas in and near liquids.

Another method for gas temperature determination is the Rayleigh scattering of photons by atoms and molecules. In this method the intensity of the scattered laser light of the plasma is compared with a reference signal with a known gas temperature in the same gas composition to determine the gas temperature of the plasma [16, 17]. However, laser diagnostics are not always available and have to be used with care in order not to change the parameters of the plasma due to, e.g., photoionization, especially for plasmas with low ionization degree and large metastable densities, which is the case for APPJs. Furthermore, this method cannot be used for helium plasma jets with air around and inside of the plasma, since the cross section of helium is low compared with air (see next sections).

The electron density can give information about the chemical reactivity of the plasma source. The broadening of atomic lines is a well-known method to determine the electron density [13, 18]. In cases of high electron densities, large gas temperatures and low pressure, other line broadening effects such as van der Waals broadening are negligible and mostly not taken into account. At the other end of the regime (low electron densities, low gas temperatures, atmospheric pressure) the van der Waals and Stark broadening are in the same order of magnitude and both have to be taken into account in the calculations, which would otherwise lead to significant overestimated electron densities or underestimated gas temperatures.

From the above it is obvious that, especially in the regimes of interest for biomedical applications, the mentioned diagnostic methods have to be used with care. This paper focuses on a direct comparison of the gas temperature, electron density and power dissipation of an RF argon and helium plasma needle. We are comparing the different diagnostics itself as well as the results obtained for the different gases and for different current root mean squares (I_{rms}) to get a detailed insight into the physical parameters of the APPJs.

This paper starts with a description of the experimental setup (section 2) and the details of the used instruments for the measurements. The next section (section 3) deals with the theoretical aspects and diagnostics we used to obtain the plasma parameters. In section 4 the results of power measurements, gas temperature and electron densities are presented. The second-to-last section (section 5), preceding the conclusion (section 6), contains a discussion of the results and an evaluation of the accuracies of the presented methods for APPJs. The morphology of the discharge is also discussed.

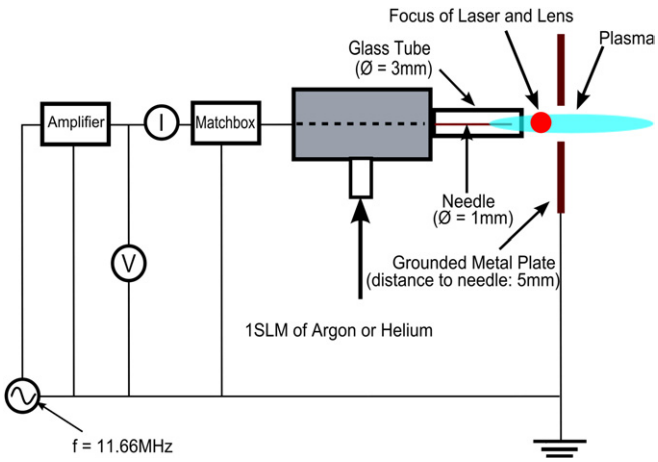

Figure 1. Experimental setup.

2. Experimental setup

Figure 1 shows a schematic of the experimental setup. The plasma source consists of an RF-driven tungsten needle with a diameter of 1 mm and a sharpened tip surrounded by a glass tube with a 3 mm outer and a 1.5 mm inner diameter. A gas flow of argon, helium or a mixture of 10% argon in helium, referred to as 'helium–argon-mix' in the following sections, is applied through the tube. The gas flow is kept constant at 1 standard litre per minute (SLM). The discharge is thus ignited in these gas compositions. The setup is not in a vacuum vessel and thus open to air. The RF frequency is 11.7 MHz generated by a signal generator (Agilent, 20 MHz Function Generator) connected to a power amplifier (Amplifier Research 75 W, 5–250 MHz). A conductance (coil) is connected in series between the high voltage output of the power amplifier and the plasma source in order to match the amplifier to the plasma source.

A grounded copper electrode is positioned at a distance of 5 mm from the needle. It has a hole with a diameter of 5 mm through which the plasma can penetrate. This electrode simulates a two-electrode system used by other research groups with a concentric electrode around the tube [11, 19, 20], while allowing access for laser spectroscopy of the active region between the two electrodes. The plasma jet is a so-called linear field plasma jet, since the electrical field and the gas flow have the same direction [21].

Voltage and current probes (Tektronix-P5100, Pearson Current Monitor-2877) are connected between the power amplifier and the matching network to an oscilloscope (Agilent Technologies, 350 MHz, 2 GSa s^{-1}). Optical emission spectroscopy and Rayleigh scattering are used for determination of the gas temperature of the active zone of the plasma. For Rayleigh scattering a YAG laser (second harmonics, 532 nm) is used and focused at around 2 mm

after the glass tube to prevent back scattering of the laser on the glass or secondary electrode. More details on the Rayleigh measurement and the used laser setup can be found in Verreycken *et al* [22].

For the line broadening and the measurements of the rotational spectra an optical fibre is used which collects the emission from the same position at which the Rayleigh measurements are performed. For the line broadening this fibre is connected to a double echelle monochromator with an Andor-CCD Camera which has a spectral resolution between 6 and 8 pm between 480 and 660 nm. For the rotational spectrum a Jobin Yvon monochromator (HR 1000 M) with a SBIG-CCD camera is used with a spectral resolution of around 22 pm which allows a broader wavelength range for single-shot measurements of molecular bands.

3. Theoretical aspects and methods

3.1. Dissipated power and power density

The average dissipated power $\overline{P}$ during one period $T = \frac{1}{f}$ can be calculated using

$$\overline{P} = \frac{1}{T}\int_0^T U(t)\cdot I(t)\,\mathrm{d}t, \qquad (1)$$

with $U(t)$ and $I(t)$ being the measured voltage and current waveforms. The disadvantage of this method is that a voltage probe introduces another capacity into the circuit. This changes the impedance of the setup and therefore strongly influences the coupling of the plasma.

To reduce these errors the voltage and current probes are connected between the power amplifier and the matching network. The drawback of this method is that the power dissipation of the matching network and the plasma is measured, rather than the power dissipation of the plasma alone.

We measured the temperature (and thus the heat dissipation in the resistance) of the coil with and without a gas flow, i.e. with and without a plasma. These measurements confirmed that the same heat dissipates in the coil with and without the plasma for the same current. This allows us to measure the power dissipation in the plasma as follows:

$$\overline{P}_{\mathrm{diss}}(I_{\mathrm{rms}}) = \overline{P}_{\mathrm{on}}(I_{\mathrm{rms}}) - \overline{P}_{\mathrm{off}}(I_{\mathrm{rms}}), \qquad (2)$$

with I_{rms} being the root mean square current, $\overline{P}_{\mathrm{diss}}$, $\overline{P}_{\mathrm{on}}$ and $\overline{P}_{\mathrm{off}}$ being the dissipated power, the power with a gas flow and the power without a gas flow, respectively. The time delay induced by the current and voltage probe is corrected for by measuring with the probes the deviation of the 90° phase shift for a known vacuum capacitor.

Figure 2 shows the measured voltage and current with and without a plasma at the same amplified current. It can be seen that the phase shift between voltage and current is reduced while the plasma is on. The reason is the decreasing capacitive nature of the load and the increasing power dissipation in the plasma, leading to a more resistive load [11].

Figure 3 shows an example of the measured power as a function of I_{rms} for a helium plasma. The power measured

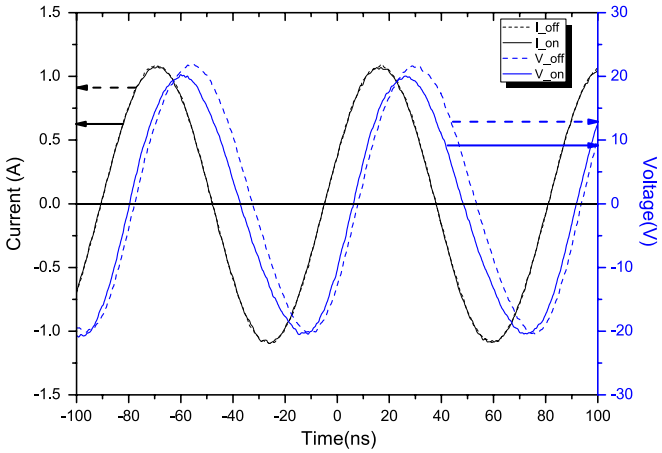

Figure 2. Measured voltage and current waveforms of the circuit with a helium plasma (I_{on}, V_{on}) and without plasma (I_{off} and V_{off}). Note that $I_{\mathrm{off}} = I_{\mathrm{on}}$.

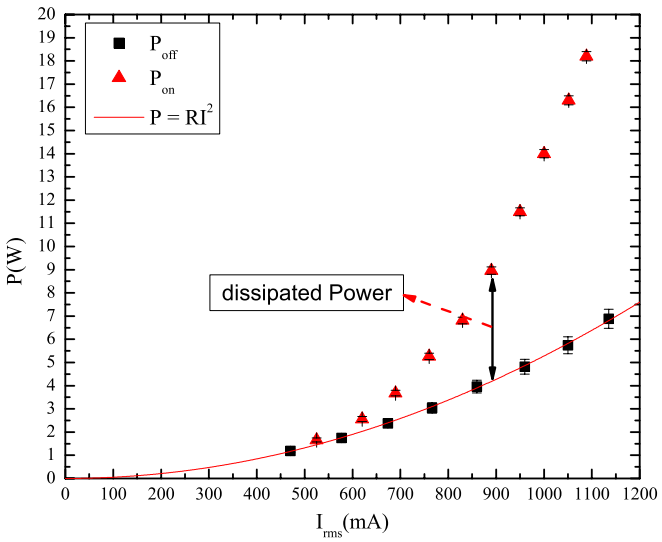

Figure 3. P_{off}, P_{on} as a function of the I_{rms} in the case of a helium plasma.

with and without a plasma is shown. Without a gas flow (and no plasma) the majority of the power dissipates in the resistive part of the coil. Fitting this power to a quadratic function reveals the I^2 dependence between power dissipation at the coil and the root mean square current as also seen by Benedikt *et al* [23].

3.2. Optical diagnostics

3.2.1. Rotational temperature. Since the discharge operates in open air, impurities, such as water, are always present in APPJ. The emission of the OH(A–X)-band is for several discharges one of the most intense emission and often used to determine the gas temperature of plasmas. With the relative intensities of the rotational bands of Q, P and R-branches of the rotational spectrum of OH(A–X)(0,0) the rotational temperature can be identified by simulating theoretical rotational spectra for different rotational temperatures (with spectra simulation programs such as Specair [24] or Lifbase

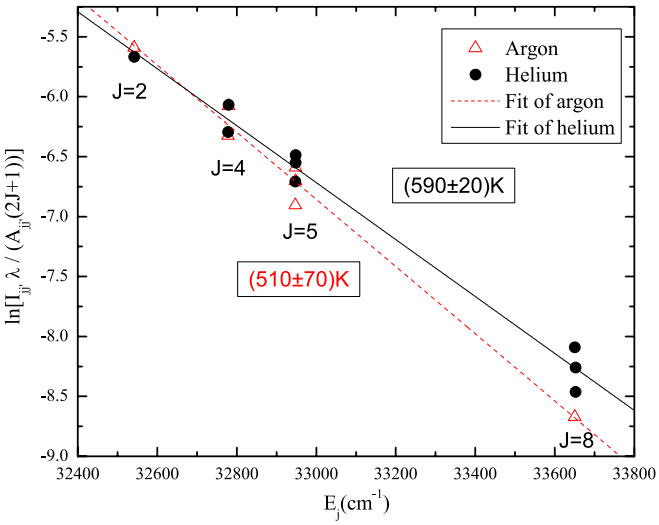

Figure 4. Boltzmann plot method for one case in argon and helium for $2 \leqslant J \leqslant 8$.

[25]). The best fit between the experiment and the simulation reveals the rotational temperature of the experiment.

These programs, however, assume a Boltzmann distribution of the rotational states in order to get a rotational temperature. This is for most atmospheric pressure plasma discharges a valid assumption, since the excited states have a large number of thermalizing collisions during their radiative lifetime, allowing the excited OH molecules to thermalize before emitting photons. Assuming that the rotational temperature is equal to the gas temperature, the gas temperature can be measured with this method.

However, previous work by Bruggeman *et al* [15, 22, 26] has shown that also in some cases for atmospheric pressure plasmas the rotational states do not follow a Boltzmann population distribution because of different population mechanisms of the rotational states and quenching which reduces the lifetime of the excited states at atmospheric pressure significantly. Note that in the case of Verreycken *et al* [22], even when the rotational population distribution was a Boltzmann distribution it could lead to an overestimate of the gas temperature.

With a high resolution spectrometer the Boltzmann plot method can be used to determine the rotational temperature. Using the relative intensities of isolated lines of the rotational spectrum, I_{rel}, and

$$I_{\mathrm{rel}} \propto \frac{A_{JJ'}(2J+1)}{\lambda_{JJ'}} \cdot \exp\left(-\frac{E_J}{kT_{\mathrm{rot}}}\right), \tag{3}$$

with $A_{JJ'}$ as the Einstein coefficient taken from [27], J and J' as the rotational quantum number of the upper and the lower states, respectively, E_J the energy of the upper level, taken from [28], k the Boltzmann constant and T_{rot} the rotational temperature, one can plot $\ln(\frac{I_{\mathrm{rel}}\lambda_{JJ'}}{A_{JJ'}(2J+1)})$ as a function of the energy E_J. If the states are Boltzmann distributed the slope yields the rotational temperature.

Figure 4 shows an example of the Boltzmann plot method for an argon and a helium case. As can be seen in the graph the values do follow a linear slope, indicating a Boltzmann distribution of the rotational states. Only isolated lines corresponding to an intensity larger than 5% of the maximum intensity are used.

For further comparison the rotational spectrum of N_2^+ (B–X)(0,0) is measured for pure helium. A best fit with simulated spectra from the program Lifbase is used to determine the rotational temperature of N_2^+.

3.2.2. Line broadening. In addition to natural broadening other effects can contribute to the broadening of emission of atoms. These broadening effects can be used to calculate plasma parameters such as the electron density and the gas temperature. However, as indicated above, at atmospheric pressure, gas temperatures close to room temperature and electron densities of around $10^{20}\,\mathrm{m}^{-3}$ the van der Waals broadening has to be taken into account, which can lead otherwise to significant overestimation of the electron density [29].

Doppler broadening. Due to the thermal motion of the particles in the plasma, the Doppler effect results in one of the broadening contributions of atomic lines. The Doppler broadening has a Gaussian line shape with a full width at half maximum (FWHM), $\Delta\lambda_{\mathrm{D}}$, of [30]

$$\Delta\lambda_{\mathrm{D}} = 7.162 \times 10^{-7}\lambda_0\sqrt{\frac{T_{\mathrm{gas}}}{M}}, \tag{4}$$

with λ_0 the wavelength in nm, T_{gas} the gas temperature in K, M the atomic mass of the emitter in atomic mass units.

Stark broadening of hydrogen lines. Due to the Coulomb interaction between the light emitting atoms and charged particles, mainly electrons, line broadening due to the Stark effect can occur. The Stark broadening results in a Lorentzian shape. In general the FWHM of the Stark broadening increases with increasing electron density [31].

To obtain the electron density the line broadening of the H_α and the H_β lines is used. For electron densities below $6 \times 10^{20}\,\mathrm{m}^{-3}$ for H_α and below $4 \times 10^{19}\,\mathrm{m}^{-3}$ for H_β fine structure has to be taken into account [32], as shown to be important by Bruggeman *et al* [33]. The limit for H_α is larger than for H_β due to the larger fine structure splitting for H_α and the smaller line broadening due to the Stark effect as for H_β at the same electron density.

Simulations of the Stark broadening of H_α for electron densities in the range 1×10^{18} to $8 \times 10^{19}\,\mathrm{m}^{-3}$ including fine structure are used to calculate the dependence between the electron density and the FWHM. For the H_β line we used simulations in the range 10^{18} to $6 \times 10^{20}\,\mathrm{m}^{-3}$ by González without inclusion of the fine structure effects [34]. However, we include *a posteriori* the effects of fine structure by fitting the theoretical spectra with a double Lorentzian profile using the simulated line broadening. These lines are folded with the fine structure of H_β which consists in first approximation of two components which are separated 8 pm from each other. We also corrected for the relative intensity of the fine structure components. This enables us to use the line broadening of H_β

for $6 \times 10^{20}\,\mathrm{m}^{-3} > n_e > 1 \times 10^{19}\,\mathrm{m}^{-3}$. From these fits we obtain the following FWHM relations, with $\Delta\lambda_S$ in nm and n_e in m^{-3}:

$$\Delta\lambda_S = 1.78 \cdot \left(\frac{n_e}{10^{23}\,\mathrm{m}^{-3}}\right)^{\frac{2}{3}} \quad \text{for } H_\alpha \quad \text{(double peak fit)}, \quad (5)$$

$$\Delta\lambda_S = 3.67 \cdot \left(\frac{n_e}{10^{23}\,\mathrm{m}^{-3}}\right)^{\frac{2}{3}} \quad \text{for } H_\beta \quad \text{(single peak fit)}. \quad (6)$$

In the case of H_β we obtained a FWHM formula for a single peak fit (with fine structure correction). Note that the correlation of H_β deviates from the standard one by 24% [35].

We also use the helium line at 667 nm to obtain the gas temperature. For this line the Stark broadening is negligible in comparison with the other contributions because of the weaker quadratic Stark effect, compared with the stronger linear Stark effect of the hydrogen atoms [30].

Resonance broadening. Interactions with neutral perturbers can be categorized in two broadening effects, i.e. the resonance broadening and the van der Waals broadening.

Resonance broadening has a Lorentzian shape and occurs when the perturber and radiator are alike and either the upper or lower transition level has an allowed transition to the ground state.

The formula for the FWHM $\Delta\lambda_R$ is, in cm, with $N = \frac{p}{k_B T_{gas}}$ in cm^{-3} and the wavelengths in cm as well,

$$\Delta\lambda_R = 8.61 \times 10^{-14} \left(\frac{g_1}{g_R}\right)^{\frac{1}{2}} \lambda_0^2 \lambda_R f_R \frac{p}{k_B T_{gas}}. \quad (7)$$

For the details of the equation the reader is referred to [30]. The resonance broadening of the helium line at 667.815 nm is one of the used methods to obtain the gas temperature. Inserting all the known values one obtains

$$\Delta\lambda_R\,(\mathrm{nm}) = \frac{26.26}{T_{gas}}. \quad (8)$$

van der Waals broadening. van der Waals broadening is another broadening effect due to neutral perturbers. The FWHM in cm can be calculated with

$$\Delta\lambda_{vdW} = 8.18 \times 10^{-26} \lambda_0^2 \left(\overline{R}^2\right)^{\left(\frac{2}{5}\right)} T_{gas}^{\frac{3}{10}} \cdot N \cdot \sum_i \left(\frac{\alpha_i^{\frac{2}{5}} \chi_i}{\mu_i^{\frac{3}{10}}}\right), \quad (9)$$

with the wavelength λ_0 in nm, μ the reduced mass in atomic mass units, the neutral particle density, N, in cm^{-3}, i = He or Ar and χ the fraction of the pertuber. For details the reader is referred to Yubero *et al* [36].

The values for the polarizability of the pertuber α are taken from [37] and for helium and argon are $2.05 \times 10^{-25}\,\mathrm{cm}^3$ and $1.64 \times 10^{-24}\,\mathrm{cm}^3$, respectively.

To include the fine structure in the calculation of the square radius a weighted average of the squared radii $\overline{R}^2$ of the seven different fine structure split levels is used. After calculating the values for the case of the atomic lines, one obtains for the FWHM

$$\Delta\lambda_{vdW}\,(\mathrm{nm}) = \frac{C}{T^{\frac{7}{10}}}. \quad (10)$$

The constant C values for the different lines and gases are presented in table 1.

Table 1. Constants for the van der Waals broadening for the different lines and gases that are used.

	Gas composition	C
$He_{667\,nm}$	Helium	1.79
H_α	Helium	2.37
	Helium–argon-mix	2.64
	Argon	5.12
H_β	Helium	2.42
	Helium–argon-mix	2.70
	Argon	5.24

Table 2. Calculated FWHMs in nm of a helium plasma with $T_{gas} = 400\,\mathrm{K}$, $p = 1$ atm and $n_e = 10^{20}\,\mathrm{m}^{-3}$.

	$\Delta\lambda_D$	$\Delta\lambda_{instr}$	$\Delta\lambda_R$	$\Delta\lambda_S$	$\Delta\lambda_{vdW}$
H_α	0.0094	0.0081		0.0178	0.0358
H_β	0.0067	0.0061		0.0367	0.0365
$He_{667\,nm}$			0.0658		0.0272

Fitting procedure. The Doppler and the instrumental broadening have a Gaussian line shape. The Stark, resonance and the van der Waals broadening have a Lorentzian shape. The convolution of these two line shapes is the so-called Voigt shape with a FWHM, $\Delta\lambda_V$, of [38]

$$\Delta\lambda_V \approx \sqrt{\left(\frac{\Delta\lambda_L}{2}\right)^2 + \Delta\lambda_G^2} + \frac{\Delta\lambda_L}{2}. \quad (11)$$

Table 2 shows calculated FWHM for pure helium for one condition. It can be seen that at these conditions van der Waals broadening is at least of the same order of magnitude as the Stark broadening for the H_α and H_β line.

To determine the gas temperature a Voigt shape is fitted to the measured lines. The Lorentzian part of the FWHM is used to estimate the gas temperature and the electron density via the van der Waals broadening and Stark broadening in case for the hydrogen lines. For the neutral helium line the sum of the resonance and van der Waals broadening is used to calculate the gas temperature.

Figures 5(*a*) and (*b*) show examples of the measured line broadenings of the H_α and H_β lines for the helium–argon mix plasma at a root mean square current of 900 mA. A two-peak Voigt fit is used for the H_α line including the effect of the fine structure as can be seen in figure 5(*a*). A single peak fit is used for the H_β line as explained in the section above.

3.2.3. Rayleigh scattering. The intensity of the Rayleigh scattered light is proportional to the particle density, n_{gas}, and the scattering cross section, σ. Considering the ideal gas law we obtain

$$I \propto \sigma n_{gas} = \sigma \frac{p}{k_B T_{gas}} \quad (12)$$

and

$$\frac{I_{ref}}{I_{meas}} = \frac{T_{gas}}{T_{ref}}, \quad (13)$$

for the same gas composition of the reference and the measurement and a constant p. Note that the Rayleigh cross sections σ for He, Ar and N_2 are $74 \times \sigma_{He} \approx 1.12 \times \sigma_{Ar} \approx \sigma_{N_2}$ [39, 40].

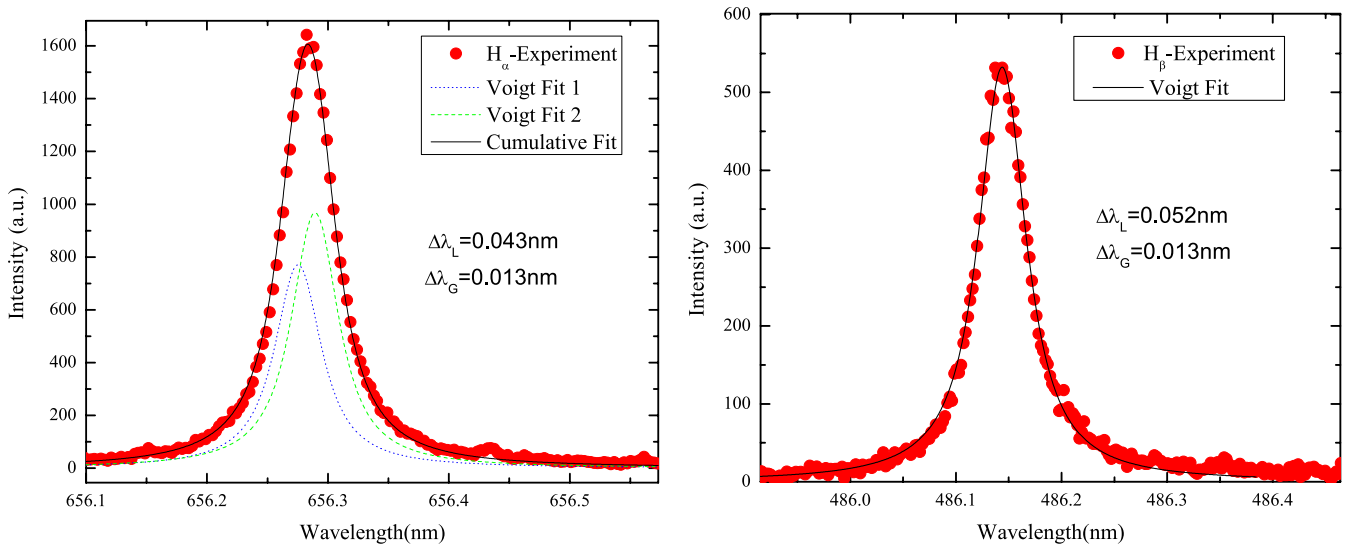

(a) Two peak fit for the H_α broadening (b) One peak fit for the H_β broadening

Figure 5. Two fit examples from the measurements of the helium–argon mix plasma of the Voigt fit for the H_α and H_β lines.

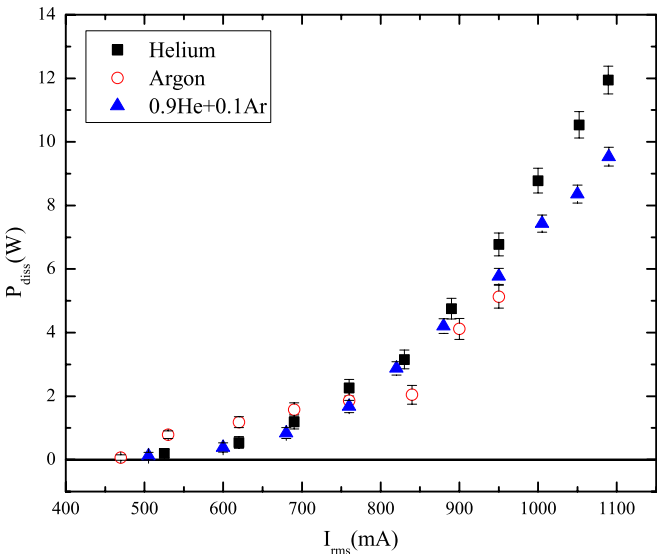

Figure 6. P_{diss} as a function of I_{rms}.

The gas temperature can be obtained by measuring a reference signal with a known gas temperature and known gas composition comparing it with the signal with the unknown temperature for the same gas composition or known gas composition.

4. Results

4.1. Power measurements

Figure 6 shows the power dissipation of the plasma for helium, argon and the helium–argon mix. It can be seen that for increasing current the power dissipation rises. The largest change in power is obtained for the helium discharge with up to 12 W for the highest amplified current. A similar increase is shown for the power dissipation with the helium–argon-mixture. The power, however, at the higher currents is lower than for helium.

Comparing these results with the power dissipation in argon one can see that at relatively low currents the power dissipation is higher in argon for the same current but it has a less steep slope at a certain regime, compared with the other cases, before it rises again until arcing occurs (at around 1 A). In the case of helium and the helium–argon-mix discharge, arcing did not occur in the measured range.

Images of the plasmas for different applied voltages are taken to estimate the volume of the plasma and to compare it with the power dissipation. Two examples for each gas for low and high currents, respectively, are shown in figures 7(*a*)–(*f*).

Figure 8 shows the estimated volume from the emission for a helium, an argon and an argon–helium mix plasma, respectively. It can be seen that for all cases the volume has approximately the same dependence to the I_{rms} as the power, showing that the power density is in first approximation constant for all investigated conditions as shown in figure 9. However, in the case of helium a small decreasing trend in the power density for increasing currents is found.

4.2. Gas temperature measurements

Figures 10(*a*)–(*c*) show the gas temperature of the different plasmas as a function of I_{rms} obtained with the different methods as discussed in section 3.2. In the case of argon (figure 10(*a*)) the line broadening of the H_α and the H_β lines, with only taking into account van der Waals broadening, Rayleigh scattering and the Boltzmann plot method for the rotational spectrum of OH, is used for the determination of the gas temperature. Assuming that Rayleigh scattering is the most accurate method to obtain the gas temperature, we compared the other methods with the results obtained by this method. It can be seen that the results obtained from the Boltzmann plot method are larger but within the error of the gas temperature obtained by Rayleigh scattering. The results from the line

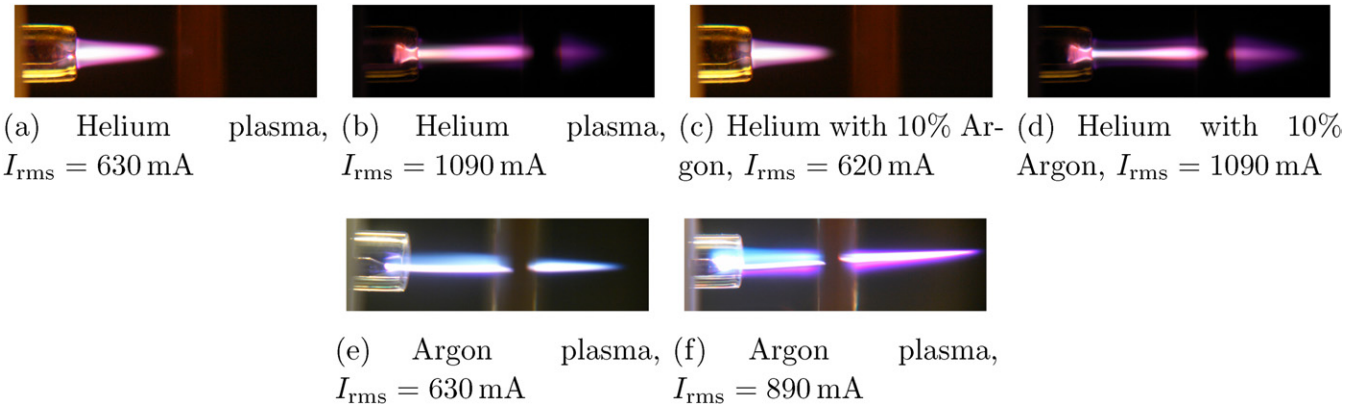

(a) Helium plasma, $I_{\mathrm{rms}} = 630\,\mathrm{mA}$ (b) Helium plasma, $I_{\mathrm{rms}} = 1090\,\mathrm{mA}$ (c) Helium with 10% Argon, $I_{\mathrm{rms}} = 620\,\mathrm{mA}$ (d) Helium with 10% Argon, $I_{\mathrm{rms}} = 1090\,\mathrm{mA}$

(e) Argon plasma, $I_{\mathrm{rms}} = 630\,\mathrm{mA}$ (f) Argon plasma, $I_{\mathrm{rms}} = 890\,\mathrm{mA}$

Figure 7. Images of the plasma for six different investigated conditions. The outer diameter of the quartz tube is 3 mm.

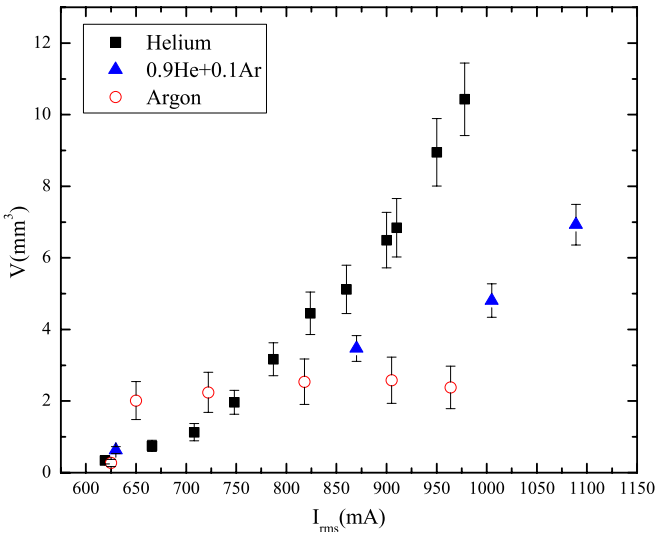

Figure 8. Estimated volume of the different discharges as a function of I_{rms}.

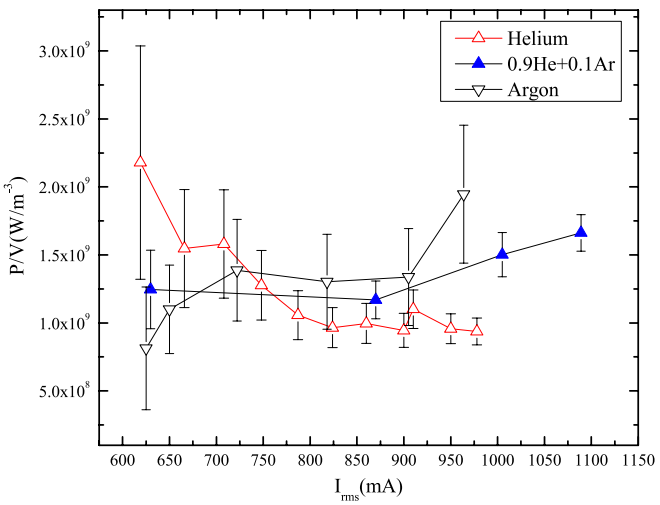

Figure 9. Estimated power density of the different discharges as a function of I_{rms}.

broadening are lower than the temperatures measured with Rayleigh scattering and the Boltzmann plot, which indicates an important contribution of the Stark broadening and a significant electron density (see the next section).

Figure 10(*b*) shows the measurements of the helium–argon mix. In addition to the methods used for the pure argon case the gas temperature is also obtained from the resonance and van der Waals broadening of a neutral helium line at 667.8 nm. It shows that the temperature obtained by the helium 667.8 nm line is consistently larger than the temperature measured with Rayleigh scattering but within the margin of error. The temperature from the H_α line broadening is, in contrast to the argon case, only slightly smaller than the temperature obtained by Rayleigh scattering. The temperature obtained by the H_β line broadening is, similar to the argon case, the smallest, which is consistent with the expected Stark broadening of these lines. The rotational temperature of the OH spectrum, however, is much larger than the gas temperature obtained by Rayleigh scattering which is clearly different than in the argon case.

Figure 10(*c*) shows the results for the helium plasma. Using the Rayleigh scattering method for pure helium is very inaccurate, since the cross section of helium is much lower than the cross section of the air around and inside the plasma, as shown in section 3.2. Furthermore, any small change in gas composition between the measurement and the reference measurement would lead to large errors in T_{gas}. Instead the rotational temperature of $N_2^+(B–X)(0,0)$ is measured. Assuming similar overestimations of the gas temperature as in case (*b*), the expected gas temperature is about 70 K lower than measured with the 667.8 nm line. As in the case for pure argon the H_α and H_β lines underestimate the gas temperature. For the rotational temperatures obtained with N_2^+ and OH it can be seen that they agree but are systematically larger than the temperatures obtained with the other methods.

4.3. Electron density

Comparing the gas temperature obtained from the van der Waals broadening of H_α and H_β in argon, helium and the helium–argon mixture, it can be seen that the obtained temperatures are in every case lower than the temperatures obtained by other methods due to the influence of the Stark broadening.

To take into account the van der Waals broadening to obtain the electron densities of the argon and argon–helium-mix plasma, the gas temperatures obtained by calculated

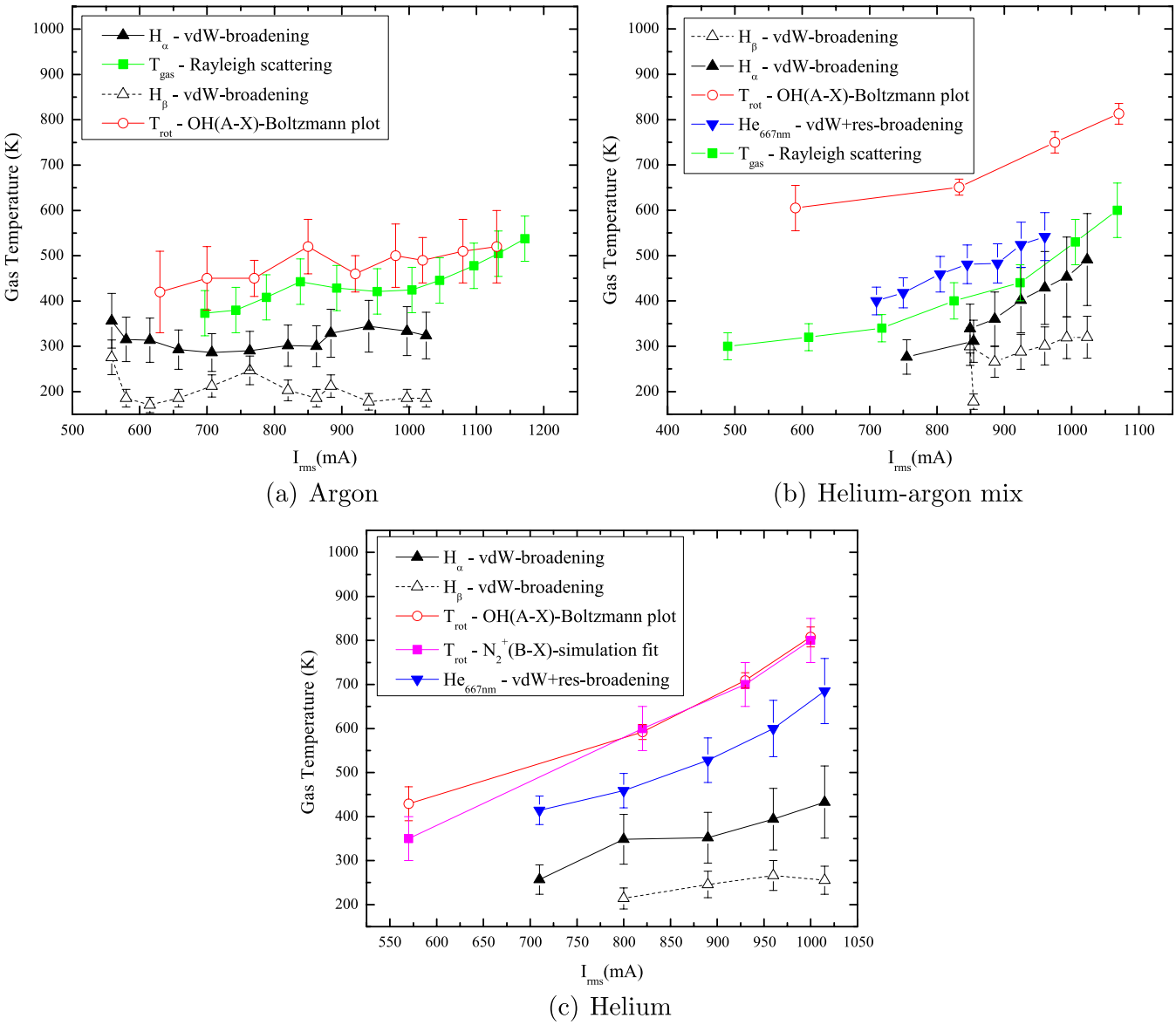

Figure 10. Gas temperature as a function of I_{rms} for the different plasmas. The Stark effect is not considered in the calculation of the temperature from the hydrogen lines in this figure.

temperatures of the Rayleigh and the line broadening of the hydrogen line measurements are compared. For helium $T_{\mathrm{He}} - 70\,\mathrm{K}$ is used, as discussed in the previous section. The difference between these temperatures is used to determine the electron density.

Figures 11(*a*)–(*c*) show the densities obtained by the Stark broadening. It can be seen that the electron density for argon is higher than in the helium and helium–argon-mix case. This is expected due to the lower ionization energy of argon compared with helium [41]. The validity and accuracy of the electron density measurements are discussed in the next section.

5. Discussion

Concerning the gas temperature diagnostics, it is clear that every method has to be used with care, in particular, in the region of interest for biomedical applications. The measurement of the gas temperature via Rayleigh scattering is, as a direct measurement of the neutral density, trustworthy, as it does not depend directly on the plasma excitation as OES results do. However, Rayleigh measurements are not always possible, such as in the case for helium plasma in air.

Optical emission spectroscopy of the rotational band of the OH(A–X)(0,0) seems to overestimate the gas temperature even though the Boltzmann plot showed no deviation of the linear slope. However, it has to be noted that only low rotational numbers have been used due to the low intensity of the discharge. A potential reason for the overestimation could be the high electron temperature in these plasma jets as shown by Bruggeman *et al* [42]. There it has been reported that in the case of helium the non-equilibrium of the OH(A) distribution increases with increased electron temperature.

We measured the rotational spectrum of $N_2(C$–$B)$ and $N_2^+(B$–$X)$ as well to obtain the gas temperature using Lifbase and Specair, assuming a Boltzmann distribution. In helium

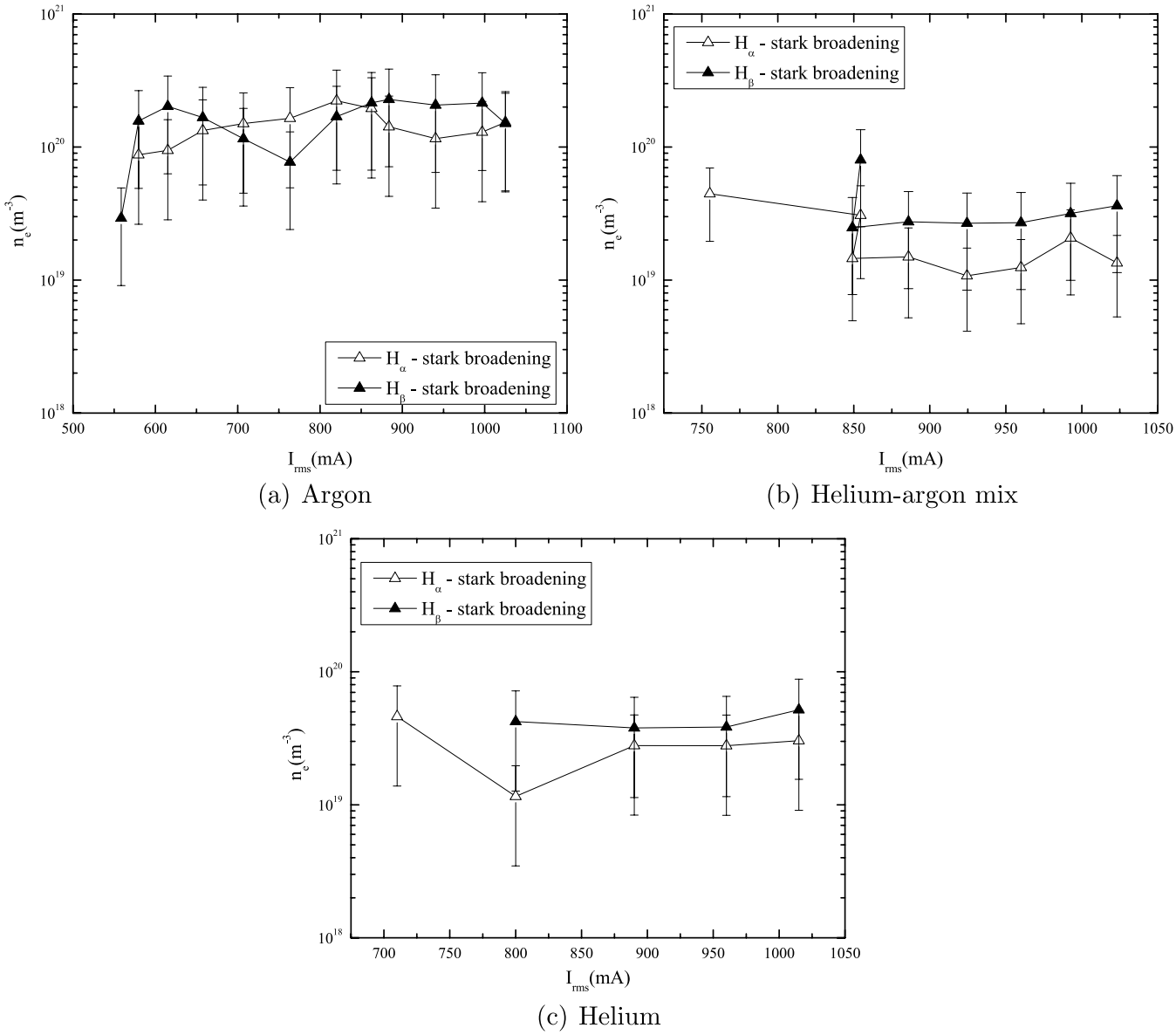

Figure 11. Electron density as a function of current root mean square for the different plasmas. The lines are shown as a guide to the eye.

$N_2(C)$ and $N_2^+(B)$ provide higher temperatures than obtained with Rayleigh scattering and the line broadening. However the obtained temperature is similar to the rotational temperature of OH(A–X) if a pure Boltzmann distribution is assumed. This is, for N_2^+, also observed in the work of Ionascut-Nedelscu *et al* [43].

In argon the temperature of $N_2(C)$ assuming Boltzmann distribution, which is not shown here, was typically above 850 K. This is due to the almost resonant energy transfer between metastables of argon to $N_2(C)$ which strongly populates high rotational states and leads to overestimations of the gas temperature [44].

A small discrepancy between the gas temperature obtained from Rayleigh scattering and the helium line at 667 nm is observed. To calculate the gas temperature we assume that the resonance broadening and the van der Waals broadening are two independent contributions to the line broadening which is in general not true since both broadening effects originate from the same perturbing atoms. This could explain the observed discrepancy in the gas temperature measurements.

The temperatures from the Rayleigh measurements show a similar dependence of the root mean square current as the volume and the power, which is a good indication that it is a good representation of the gas temperature. Similar trends have been found in the work of Verreycken *et al* for discharges of 2500–3500 K [22]. It has to be noted that even though the temperatures range from 300 to 600 K, depending on the gas, the gas temperature at the end of the jet is smaller than the temperature in the active region of the plasma as is estimated from gas temperature measurements by temperature strips. These measurements yield temperatures between 300 to 350 K at the tip of the plasma at powers of around 1 W or a few centimetres away from the plasma at higher power. This shows that in spite of the reported temperatures up to 600 K in the core the APPJ can be used for heat-sensitive applications.

The obtained rotational temperature of OH(A) always seems largest compared with the other temperature measurements. We now estimate the gas temperatures upper limit from a simple power balance of the plasma, assuming that all power is converted in gas heating and all heat is removed by the forced flow.

This leads to

$$P = \frac{\Delta m}{\Delta t} c \cdot \Delta T, \tag{14}$$

with power $P = 3\,\mathrm{W}$, heat capacity $c = 5193\,\mathrm{J\,kg^{-1}\,K^{-1}}$ and mass flow $\frac{\Delta m}{\Delta t} = 3 \times 10^{-6}\,\mathrm{kg\,s^{-1}}$. This shows that the gas temperature cannot exceed 500 K at 3 W which corresponds to 800 mA in helium, while the rotational temperature of OH(A) is (600 ± 50) K in this case. It is thus clearly an overestimate of the gas temperature.

Measurements of the electron density clearly show that $n_e^{He} < n_e^{Ar}$. In all cases the electron density is approximately constant for all currents, which is to be expected since the power density is, to first order, constant. Furthermore, the strong influence of the van der Waals broadening is clear, as for the reported conditions the van der Waals broadening is on the same order of magnitude as or larger than the Stark broadening. This means that the accuracy of the electron density measured with Stark broadening is determined by the accuracy of the gas temperature since

$$\Delta\lambda_S = \Delta\lambda_L - \left(\frac{C}{T^{0.7}}\right). \tag{15}$$

This leads, e.g. for the H_α in helium at $T = 400\,\mathrm{K}$ with an error of $\Delta T = 100\,\mathrm{K}$, to an uncertainty of 4 pm for the FWHM of the Voigt fit which corresponds to an uncertainty of $\Delta n_e \approx 2.5 \times 10^{19}\,\mathrm{m^{-3}}$.

Clearly only an order of magnitude estimation can be obtained for the electron densities for low temperature atmospheric pressure plasmas with this method. For low ionized plasmas such as the helium discharge the presented results are an upper limit.

Since the main electron energy loss is due to elastic collisions in the plasma jet, a simple power balance equation can be used to obtain an independent estimation of the electron density with

$$\frac{P}{V} \approx n_e \cdot n_{He} \cdot \frac{3}{2} k^{el} \cdot \left(T_e - T_g\right) \cdot 2 \cdot \frac{m_e}{m_{He}}. \tag{16}$$

Using an elastic collision rate, k^{el}, of $0.6 \times 10^{-13}\,\mathrm{m^3\,s^{-1}}$ obtained from Bolsig+ [45], a helium density, n_{He}, of $2.5 \times 10^{25}\,\mathrm{m^{-3}}$ and an estimated electron temperature, T_e, of 3 eV the formula can be rewritten as

$$\frac{P}{V} \approx 2.48 \times 10^{-10} n_e. \tag{17}$$

With an obtained power density of $(1.2 \pm 0.4) \times 10^9\,\mathrm{W\,m^{-3}}$ the estimated electron density is

$$n_e = (4.0 \pm 1.3) \times 10^{18}\,\mathrm{m^{-3}}. \tag{18}$$

Table 3. Timescales of diffusion and dissociative recombination.

Gas	t_{diss} (s)	t_{diff} (s)
Helium	10^{-6}–10^{-5}	10^{-6}
Argon	10^{-8}	10^{-5}

Showing that the estimate of n_e seems to be more accurate than the line broadening measurements. An additional contribution to the experimental line broadening can be induced by the electrical field in the plasma (see, e.g., [46]). This could be especially important in the case of helium. The Holtsmark electrical field [13] for n_e smaller than $10^{-19}\,\mathrm{m^{-3}}$ is equal to or smaller than $100\,\mathrm{V\,cm^{-1}}$. The electrical field in a helium discharge of 3 eV is in the local field approximation about $250\,\mathrm{V\,cm^{-1}}$ [45] thus in the same order of magnitude as the Holtsmark electric field.

Comparing the shape of the different plasmas it is clear that the argon discharge is more radially contracted than the helium discharge. In many cases thermal ionization instabilities can explain these contractions [47, 48]. However, for thermal instabilities the temperature in the bulk is on the order of thousand kelvin or more. Considering the obtained gas temperatures of the plasma source, thermal instabilities are unlikely.

We compare the timescales of diffusion and dissociative recombination including helium, argon, nitrogen and oxygen. The timescale of dissociative recombination is estimated with

$$\tau_{diss} = \frac{1}{n_e k_{ei}}, \tag{19}$$

with k_{ei} being the electron–ion recombination, taken from [49]. The timescale of diffusion is estimated with

$$\tau_{diff} = \frac{\Lambda^2}{D}, \tag{20}$$

with $\Lambda = R/2.4 \approx 0.1\,\mathrm{mm}$ being the geometric constant with R being the radius of the plasma, $D = \frac{\mu k T_e}{e}$ the diffusion, with kT_e assumed to be maximally 3 eV as the electron temperature and μ as the ion mobility taken from Ellis *et al* [50].

Table 3 shows the results of the calculation. The estimates are valid for the following ions: N_2^+, O_2^+, He_2^+ and Ar_2^+. It shows that in the case of argon the dissociative recombination is much faster than the diffusion. The local electron loss results in a contracted shape of the discharge in the case of argon. In the case of the helium discharge diffusion losses are faster than or equal to recombination losses, which is in agreement with the more diffuse shape of the plasma. A similar effect has also recently been reported in atmospheric pressure microwave plasmas [51].

6. Conclusion

We obtained different plasma parameters of a helium and an argon cold APPJ operating in open air. The power dissipation of the plasma was measured with electrical probes, with corrections of the power dissipation in the matching box. The power dissipation ranged from 100 mW to 12 W for the pure

helium plasma and up to 6 W in the case of the argon plasma. It was shown that the discharges in the investigated range had in first approximation a constant power density.

The gas temperature was obtained by Rayleigh scattering, the rotational spectrum of the OH(A–X)(0,0) transition and line broadening. The rotational temperature seemed, in the case of helium and the helium–argon mixture, to be an overestimation of the gas temperature. The measured gas temperature of the helium plasma ranged between 300 to 600 K for different I_{rms} from 500 to 1100 mA. The gas temperature of the argon plasma was in the range 380 to 450 K.

The Stark broadening of H_α and H_β was used to estimate the electron density of the discharges. The results showed that the helium plasma had a density of around $(3.4 \pm 2.5) \times 10^{19}\,\mathrm{m}^{-3}$ while in the argon discharge the value was around $(1.1 \pm 0.7) \times 10^{20}\,\mathrm{m}^{-3}$. A power balance estimate in the case of the helium plasma provided a more accurate electron density of $(4.0 \pm 1.3) \times 10^{18}\,\mathrm{m}^{-3}$ compared with the line broadening method due to the important contribution in the experimental line profile of the van der Waals broadening and inaccuracy in the gas temperature.

With the obtained results the radial contraction of the argon plasma, compared with the more diffuse helium plasma, was explained by determining the dominant charge loss mechanisms. It had been shown that dissociative recombination processes occur much faster than diffusion, hence leading to a more contracted plasma in argon. For helium charge losses are dominantly diffusive explaining the more diffuse shape of the helium discharge.

Acknowledgments

The authors would like to thank M Á González for providing the simulated line profiles of H_α and H_β. P Bruggeman acknowledges funding from STW (Dutch Technology Foundation). This work is partly supported by the research program of the Foundation for Fundamental Research on Matter (FOM), which is part of the Netherlands Organization for Scientific Research (NWO).

References

[1] Lloyd G, Friedman G, Jafri S, Schultz G, Fridman A and Harding K 2010 *Plasma Process. Polym.* **7** 194–211
[2] Laroussi M 2009 *IEEE Trans. Plasma Sci.* **37** 714–25
[3] Ehlbeck J, Schnabel U, Polak M, Winter J, von Woedtke T, Brandenburg R, von dem Hagen T and Weltmann K D 2011 *J. Phys. D: Appl. Phys.* **44** 013002
[4] Laroussi M and Akan T 2007 *Plasma Process. Polym.* **4** 777–88
[5] Bárdos L and Baránková H 2010 *Thin Solid Films* **518** 6705–13
[6] Kong M G, Kroesen G M W, Morfill G, Nosenko T, Shimizu T, v Dijk J and Zimmermann J L 2009 *New J. Phys.* **11** 115012
[7] Schütze A, Jeong J Y, Babayan S E, Park J, Selwyn G S and Hicks R F 1998 *IEEE Trans. Plasma Sci.* **26** 1685–94
[8] Tümmel S, Mertens N, Wang J and Viöl W 2007 *Plasma Process. Polym.* **4** S465–9
[9] Godyak V A and Piejak R B 1990 *J. Vac. Sci. Technol.* A **8** 3833–7
[10] Kim D B, Rhee J K, Moon S Y and Choe W 2006 *Appl. Phys. Lett.* **89** 061502
[11] Yanguas-Gil A, Focke K, Benedikt J and von Keudell A 2007 *J. Appl. Phys.* **101** 103307
[12] Léveillé V and Coulombe S 2005 *Plasma Sources Sci. Technol.* **14** 467–76
[13] Griem H R 1997 *Principles of Plasma Spectroscopy* (Cambridge : Cambridge University Press)
[14] Laux C O, Spence T G, Kruger C H and Zare R N 2003 *Plasma Sources Sci. Technol.* **12** 125–38
[15] Bruggeman P, Iza F, Guns P, Lauwers D, Kong M G, Gonzalvo Y A, Leys C and Schram D C 2010 *Plasma Sources Sci. Technol.* **19** 015016
[16] Marshall K A and Hieftje G M 1987 *J. Anal. At. Spectrom.* **2** 567–71
[17] Rousseau A, Teboul E, v d Sande M J and v d Mullen J J A M 2002 *Plasma Sources Sci. Technol.* **11** 47–52
[18] Kelleher D E, Wiese W L, Helbig V, Greene R L and Oza D H 1993 *Physica Scri.* **T47** 75–79
[19] Förster S, Mohr C and Viöl W 2005 *Surf. Coat. Technol.* **200** 827–30
[20] Foest R, Kindel E, Lange H, Ohl A, Stieber M and Weltmann K D 2007 *Contrib. Plasma Phys.* **47** 119–28
[21] Walsh J L and Kong M G 2008 *Appl. Phys. Lett.* **93** 111501
[22] Verreycken T, van Gessel A F H, Pageau A and Bruggeman P 2011 *Plasma Sources Sci. Technol.* **20** 024002
[23] Benedikt J, Raballand V, Yanguas-Gil A, Focke K and von Keudell A 2007 *Plasma Phys. Control. Fusion* **49** B419–27
[24] Laux C 2002 Radiation and nonequilibrium collisional-radiative models *Physico-Chemical Modeling of High Enthalpy and Plasma Flows (Rhode-Saint-Genèse, Belgium, 4–7 June 2002)* (von Karman Institute Special Course) ed D Fletcher *et al*
[25] Luque J and Crosley D R 1999 *SRI International Report MP 99-009*
[26] Bruggeman P, Schram D C, Kong M G and Leys C 2009 *Plasma Process. Polym.* **6** 751–762
[27] Chidsey I L and Crosley D R 1980 *J. Quant. Spectrosc. Radiat. Transfer* **23** 187–199
[28] Dieke G H and Crosswhite H M 1962 *J. Quant. Spectrosc. Radiat. Transfer* **2** 97–199
[29] Schäfer J, Sigeneger F, Foest R, Loffhagen D and Weltmann K D 2010 *Eur. Phys. J.* D **60** 531–538
[30] Djurović S and Konjević N 2009 *Plasma Sources Sci. Technol.* **18** 035011
[31] Gigosos M A, González M A and noso V C 2003 *Spectrochim. Acta* B **58** 1489–504
[32] Olchawa W, Olchawa R and Grabowski B 2004 *Eur. Phys. J.* D **28** 119–124
[33] Bruggeman P, Schram D C, González M A, Rego R, Kong M G and Leys C 2009 *Plasma Sources Sci. Technol.* **18** 025017
[34] González M A 2010, private communication
[35] Gigosos M A, González M A and Cardeñoso V 2003 *Spectrochim. Acta* B **58** 1489–504
[36] Yubero C, Dimitrijević M S, García M C and Calzada M D 2007 *Spectrochim. Acta* B **62** 169–76
[37] Allen C W 2000 *Allen's Astrophysical Quantities* 4th edn (London: The Athlone Press)
[38] Whiting E E 1968 *J. Quant. Spectrosc. Radiat. Transfer* **8** 1379–84
[39] Palomares J M, Iordanova E I, Gamero A, Sola A and v d Mullen J J A M 2010 *J. Phys. D: Appl. Phys.* **43** 395202
[40] Murphy A B and Farmer A J D 1992 *J. Phys. D: Appl. Phys.* **25** 634–43
[41] Jonkers J, v d Sande M, Sola A, Gamero A and v d Mullen J A M 2003 *Plasma Sources Sci. Technol.* **12** 30–8
[42] Bruggeman P, Verreycken T, González M A, Walsh J L, Kong M G, Leys C and Schram D C 2010 *J. Phys. D: Appl. Phys.* **43** 124005

[43] Ionascut-Nedelcescu A, Carlone C, Kogelschatz U, Gravelle D V and Boulos M I 2008 *J. Appl. Phys.* **103** 063305
[44] Ngyuen T D and Sadeghi N 1983 *Chem. Phys.* **79** 41–55
[45] Hagelaar G J M and Pitchford L C 2005 *Plasma Sources Sci. Technol.* **14** 722–33
[46] Wujec T, Janus H W and Jeleński W 2003 *J. Phys. D: Appl. Phys.* **36** 868–77
[47] Chalmers I D 1971 *J. Phys. D: Appl. Phys.* **4** 1147–51
[48] Raizer Y P 1991 *Gas Discharge Physics* (Berlin: Springer)
[49] Fridman A 2008 *Plasma Chemistry* (New York: Cambridge University Press)
[50] Ellis H W, Pai P Y, McDaniel E W, Mason E A and Viehland L A 1976 *At. Data Nucl. Data Tables* **17** 177
[51] Castaños-Martínez E, Moisan M and Kabouzi Y 2009 *J. Phys. D: Appl. Phys.* **42** 012003